Gavrilov et al. Earth, Planets and Space (2015) 67:86
DOI 10.1186/s40623-015-0259-2

Earth, Planets and Space
a SpringerOpen Journal

FULL PAPER Open Access

Simulating influences of QBO phases and orographic gravity wave forcing on planetary waves in the middle atmosphere

Nikolai M. Gavrilov[1*], Andrej V. Koval[1*], Alexander I. Pogoreltsev[2] and Elena N. Savenkova[1,2]

Abstract

Recently developed parameterization of stationary orographic gravity waves (OGWs) generated by the Earth's topography was implemented into a general circulation model of the middle and upper atmosphere. We performed numerical simulations of the zonal mean wind and amplitudes of stationary planetary waves and normal atmospheric modes with periods of 4–16 days at altitudes from the troposphere to the lower thermosphere in January for easterly and westerly phases of the quasi-biennial oscillation (QBO) including and excluding the stationary OGW parameterization. Simulations show that accounting dynamical and thermal effects of stationary OGWs can lead to substantial changes (up to 50–90 %) in the amplitudes of stationary planetary waves. Amplitudes of westward travelling normal atmospheric modes change (up to 50–90 %) at different altitudes and latitudes of the northern hemisphere due to OGW effects. Transitions from the easterly to westerly QBO phases can change planetary wave amplitudes up to ±30–90 % at middle and high latitudes. These changes in PW amplitudes are consistent with distributions of EP-flux and refractive index under different QBO phases simulated including our parameterization of stationary OGWs.

Keywords: Middle and upper atmosphere; Circulation modeling; Planetary waves; Orographic gravity waves; Wave heating; Parameterization; Quasi-biennial oscillation

Background

Energy and momentum transport by internal atmospheric waves is an important factor of dynamical interactions between the lower and upper atmosphere and a substantial contributor to space weather developments (Kelley 1997). It is important for the numerical modeling of the general circulation and thermal regime of the middle and upper atmosphere to account for accelerations of the mean flow and heating rates produced by dissipating internal waves (Holton 1975). One of the major sources of mesoscale atmospheric waves is the Earth's topography (Gossard and Hooke 1975). Generation of orographic gravity waves (OGWs) at the surface and their propagation into the middle and upper atmosphere significantly affect the atmospheric general circulation as well as the amplitudes and other parameters of planetary waves in these regions. Simplified algorithms parameterizing thermal and dynamical effects of orographic waves have been developed (e.g., Kim and Arakawa 1995; Lott and Miller 1997; Scinocca and McFarlane 2000; Vosper and Brown 2007; Catry et al. 2008; Geller et al. 2011). Recently, Gavrilov and Koval (2013) developed a new parameterization of dynamical and thermal effects of OGWs generated by the surface topography and propagating into the middle and upper atmosphere.

An essential condition for calculating vertical profiles of wave accelerations of the mean flow and heating rates is to take into account the rotation of the atmosphere, which may substantially influence the characteristics of stationary OGWs with ground-based observed frequencies $\sigma = 0$. The surface topography and jet streams in the troposphere are distributed over the globe, and wave sources in the atmosphere vary seasonally, thus leading to differences in wave characteristics between winter and summer hemispheres (e.g., Gavrilov and Fukao 1999). Satellite measurements identified substantial inhomogeneity of latitude–longitude distributions of

* Correspondence: gavrilov@pobox.spbu.ru; koval_spbu@mail.ru
[1]Atmospheric Physics Department, Saint-Petersburg State University, Saint-Petersburg 198504, Russia
Full list of author information is available at the end of the article

orographic wave characteristics in the middle atmosphere, which depend significantly on season (Eckermann and Preusse 1999; Preusse et al. 2002; Jiang et al. 2002; Smith et al. 2009; Gavrilov 2007). Therefore, it is essential to account for observable inhomogeneities of the wave sources in numerical general circulation models of the middle atmosphere. Some of such numerical studies of gravity wave influence on the general circulation, amplitudes, and seasonal variations of tides were performed, for instance, by McLandress (2002), Gavrilov et al. (2005), Ortland and Alexander (2006), and Watanabe and Miyahara (2009). Inhomogeneities of gravity wave sources and propagation conditions in the middle atmosphere may lead to the generation of planetary waves with variable characteristics (e.g., Holton 1984; Mayr et al. 2011; Hoffmann et al. 2012).

Gavrilov et al. (2013a) implemented a parameterization of dynamical and thermal effects of stationary OGWs generated by the surface topography into a numerical model of general circulation at altitudes from the troposphere up to the lower thermosphere. They showed that stationary OGWs produce substantial changes in the general atmospheric circulation of the middle and upper atmosphere. Gavrilov et al. (2013b) simulated changes in the amplitudes of atmospheric planetary waves (PWs) caused by stationary OGWs. They considered mainly PW modes generated in the general circulation model itself due to linear and nonlinear interactions.

In the present study, we extended the simulations of stationary OGW impacts on the general circulation and PWs in the middle and upper atmosphere. We improved parameterizations of the travelling normal atmospheric mode (NAM) forcing in the general circulation model and simulated different modes of stationary PWs and travelling NAMs taking into account dynamical and heating effects of stationary OGWs. It is assumed that the quasi-biennial oscillations (QBOs) of the zonal mean flow at lower latitudes at stratospheric heights can affect PW propagation conditions (e.g., Baldwin et al. 2001). Therefore, we performed numerical experiments for the background and initial conditions typical for the westerly and easterly QBO phases. In this paper, we focus on the changes in amplitudes of stationary PWs and travelling NAMs in the atmosphere due to OGW effects under different QBO phases.

Methods

Flow over the mountains is an important source of OGWs in the atmosphere. In this study, we use the parameterization of dynamical and thermal effects of stationary OGWs described in detail by Gavrilov and Koval (2013). To calculate vertical profiles of total vertical wave energy flux and associated accelerations of horizontal components of wind by stationary OGWs with ground-based observed frequencies $\sigma = 0$, we used wave polarization relations taking into account the rotation of the atmosphere. Propagations of such OGWs in the dissipative heterogeneous atmosphere lead to momentum and energy exchanges between the mean flow and waves and to heating of the atmosphere due to wave energy dissipation. To describe correctly the energy balance of the considered dynamical processes, we used analytical relations between the rate of wave energy dissipation and wave acceleration for nonzero vertical gradients of the mean wind.

Conventional theory of atmospheric acoustic-gravity waves (AGWs) in flat rotating atmosphere (e.g., Gossard and Hooke 1975) provides polarization relations. They may be simplified for stationary AGWs with frequency $\sigma = 0$ and large vertical $|m| >> 1/(2H)$ and horizontal $k^2 >> (f/c)^2$ wave numbers (where f is the Coriolis parameter, c is the sound speed, and H is the atmospheric density scale height). AGW polarization relations show that the amplitude U of velocity variations v_k along axis x_k parallel to horizontal wave vector $\boldsymbol{k}$ is much larger than the amplitude V of velocity fluctuations in the perpendicular direction. In this case, Gavrilov and Koval (2013) obtained the following expressions for total vertical wave energy flux F_E, for wave acceleration a_{wk} along axis x_k, and for total heating rate ε_w produced by stationary OGWs:

$$\begin{aligned} F_E &= -\frac{\bar{\rho} f^2 U^2}{2mk\bar{\nu}_k}; \quad m^2 = \frac{N^2}{\bar{\nu}_k{}^2}\left(1-\frac{f^2}{k^2\bar{\nu}_k{}^2}\right)^{-1}. \\ a_{wk} &= -\frac{m^2 U^2}{2\bar{\nu}_k}(\nu + K_z)\left(1+\frac{1}{(\gamma-1)\,\mathrm{Pr}}\right), \\ \varepsilon_w &= (\nu + K_z)\delta m^2 U^2, \end{aligned} \tag{1}$$

where N is the Brunt-Väisälä frequency; ν and K_z are the kinematic coefficients of molecular and turbulent viscosity, respectively; δ is a factor depending on the vertical gradients of the mean wind (see Gavrilov and Koval 2013); and Pr is the effective Prandtl number. When $\delta = 1$, the expression for ε_w in Eq. (1) corresponds to the expression for the wave energy dissipation rate caused by molecular and turbulent viscosity. One can find the altitude profile of U^2 from the approximate equation (see Gavrilov and Koval 2013) having the following form:

$$\frac{\partial}{\partial z}\left(\frac{\bar{\rho} f^2 U^2}{2|k|N}\sqrt{1-\frac{f^2}{k^2\bar{\nu}_k{}^2}}\right) = -\bar{\rho}(\nu + K_z)\delta m^2 U^2. \tag{2}$$

One can solve this equation relative to U^2 for specified wave amplitude at the lower boundary and given vertical profiles of the mean temperature, wind, molecular and turbulent viscosity, and heat conduction (see Gavrilov and Koval 2013; Gavrilov and Yudin 1992). Then one can use Eq. (1) to calculate OGW total heating rates and wave accelerations, which can parameterize the thermal

and dynamical effects of these waves in atmospheric general circulation models.

To parameterize mesoscale topography, we used a modification of the method developed by Scinocca and McFarlane (2000), which implies the concept of "subgrid orography." It takes into account height variations of the Earth's surface with horizontal scales smaller than horizontal grid spacing of the used numerical model. We extracted the so-called subgrid topography utilizing low- and high-frequency numerical filtering of the realistic horizontal distributions of the surface relief (Gavrilov and Koval 2013). Near each grid point, we used an elliptical approximation of the filtered subgrid-scale surface heights (Lott and Miller 1997). At the low boundary, we determine OGW amplitude and effective horizontal wave number using the analysis of forces affecting the atmospheric flow moving over the effective elliptical mountain barrier developed by Phillips (1984). These results are required to determine the vertical profiles of wave accelerations and heat fluxes (see Gavrilov and Koval 2013). For practical realization of our OGW parameterization, we used the ETOPO2 (2015) database of the Earth's surface elevations with resolution of two angle minutes along latitude and longitude.

To take into account the OGW influence on atmospheric dynamics, the above-mentioned parameterization was implemented into the middle and upper atmosphere general circulation model (MUAM) described by Pogoreltsev (2007) and Pogoreltsev et al. (2007). The starting point for this model was the COMMA general circulation model developed in Cologne University, Germany (e.g., Jakobs et al. 1986; Ebel et al. 1995). The MUAM solves the standard set of hydrodynamic equations in spherical coordinates. Calculations are carried out for altitudes from the ground up to about 135 km, but the weather changes and cloudiness in the troposphere are not included. The regular horizontal grid spacing in the model is 5.6° along longitude and 5° in latitude. The vertical grid was equidistantly spaced in the log-pressure coordinate $z = H^*\ln(p_0/p)$, where p_0 is the surface pressure and $H = 7$ km is the mean density scale height. Up to 100 km, this coordinate approximately corresponds to the geopotential height. In the present simulations, we used the MUAM version with 48 vertical levels (separated by 2.8 km) and with the 450-s integration time step. For PW analysis in this study, we used model outputs every 4 h.

In the lower atmosphere, the MUAM uses climatological geopotential height and temperature from the UK Met Office model (Swinbank and O'Neill 1994) averaged over years 1992–2011 for January. In addition, we used three-dimensional ozone distributions in the middle atmosphere taking account of climatological (averaged for years 1996–2005) longitudinal inhomogeneities (Suvorova and Pogoreltsev 2011). Besides stationary planetary waves, the MUAM can reproduce travelling modes (Pogoreltsev et al. 2014). As far as the MUAM does not reproduce tropospheric weather, we parameterize tropospheric sources of westward travelling normal atmospheric modes (NAMs) with additional terms in the heat balance equation of the model, which consist of sets of time-dependent sinusoidal components with periods equivalent to the NAMs with zonal wavenumbers $m = 1$ and $m = 2$. These components have latitude structures corresponding to the respective Hough functions calculated using the algorithm by Swarztrauber and Kasahara (1985). Specified NAM periods are equal to the periods of a resonant atmospheric reaction to the low-altitude wave forcing determined with a linear PW model by Pogoreltsev (1999). The present MUAM version takes into account the NAMs (1,1), (1,2), (1,3), (2,1), and (2,2) within the classification proposed by Longuet-Higgins (1968), which have resonant periods of 120, 220, 360, 90, and 170 h, respectively. In the present sensitivity study, we used the same amplitudes (2×10^{-5} K/s) of the wave heat sources at altitude 10 km for all the above-mentioned NAMs. These heating rates produce simulated NAM amplitudes in the stratosphere approximately corresponding to the observed ones (Pogoreltsev et al. 2009).

Important features of the middle atmosphere dynamics are the quasi-biennial oscillation (QBO) of zonal wind at low latitudes (Baldwin et al. 2001). To reproduce them in the MUAM, Pogoreltsev et al. (2014) proposed to use an additional term in the momentum equation for zonal wind velocity, which is proportional to the difference between calculated and observed zonal mean winds at latitudes from 17.5° S to 17.5° N and altitudes from 0 up to 50 km.

To subdivide westerly and easterly QBO phases in earlier papers (e.g., Holton and Tan 1980; Yamashita et al. 2011; Inoue et al. 2011), directions of eastward and westward winds observed in the equatorial stratosphere at pressure levels 50–70 hPa were used. Huesmann and Hitchman (2001) analyzed QBO using NCEP reanalysis data and showed that climatological mean zonal winds and their annual cycles may produce asymmetries in durations of descending zones of easterly and westerly QBO winds. To diminish these asymmetries, Huesmann and Hitchman (2001) proposed the usage of the equatorial zonal wind shear anomaly index calculated from zonal wind differences at two heights in the stratosphere. To eliminate asymmetries in the easterly and westerly wind zones, Pogoreltsev et al. (2014) proposed calculating of differences between monthly mean for each year and climatological (averaged over years 1992–2011) zonal wind velocities over the equator at the altitude of 30 km. Positive and negative differences correspond to the westerly and easterly QBO phases.

Pogoreltsev et al. (2014) found the maximum variability of QBO winds at altitudes near 30 km (pressure levels 10–20 hPa) and determined the westerly and easterly wind zones at those heights. Such procedure gives the same years of the easterly and westerly QBO phases as those obtained by Inoue et al. (2011). Westerly and easterly QBO wind zones have wavelike structures versus altitude with vertical wavelengths about 20 km (e.g., Baldwin et al. 2001; Huesmann and Hitchman 2001). Therefore, the timing of the westerly and easterly winds very much depends on the altitudes of their determination. Hence, the westerly and easterly QBO zones determined at pressure levels 10–20 hPa may have substantial phase shifts compared to the same zones obtained at 50–70 hPa, and even opposite wind directions at these levels are often supposed (e.g., Giorgetta et al. 1999; Krismer and Giorgetta 2014). Such vertical phase shifts one should keep in mind, when comparing QBO phases determined at different altitudes and pressure levels. Pogoreltsev et al. (2014) selected years with the westerly and easterly QBO phases at altitude 30 km (10–20 hPa) and calculated the average zonal mean distributions of zonal wind and temperature for both QBO phases at latitudes from 17.5° S to 17.5° N and altitudes from 0 up to 50 km, which we use in the present analysis.

According to Pogoreltsev et al. (2007), the equation of heat balance in the MUAM contains additional terms proportional to differences between the calculated and observed zonal mean temperatures in the troposphere and lower stratosphere to improve the simulation of the tropospheric jets. The used values of proportionality factors in these additional terms for zonal wind velocity and temperature correspond to a 5-day relaxation interval to nudge the calculated zonal wind and temperature to the observed values.

The numerical modeling starts from an initial windless state with vertical temperature distribution taken from the MSISE model (Hedin 1991) for January. During the first days of simulations, we perform several stages of "adjustment." In the first 30 model days, we use constant values of geopotential height at the lower boundary and do not include the OGW parameterization. The observed variations of geopotential heights and OGW parameterization are involved after the 30th day of calculations. During the first 120 days, the model performs calculations using only the daily averaged heating rates, and then daily variations of heating are gradually included. After the 120th model day, the MUAM uses an additional prognostic equation for the geopotential at the lower boundary. The calculations after the 330th model day take into account seasonal changes in solar heating. Starting dates for the calculations in our study were adjusted such that the model days 330–390 correspond to January–February, when PW and NAM amplitudes are maximum in the northern hemisphere.

Results

We used the above-described MUAM with included OGW dynamical and thermal effects to simulate the changes in PW and NAM characteristics caused by orographic waves generated near the Earth's surface. Calculations correspond to conditions averaged for Januaries with the easterly and westerly QBO phases over years 1992–2011 (see "Methods").

Altitude-latitude structure of zonal mean wind and OGW

Figure 1a shows the simulated monthly mean zonal wind averaged over longitude for January at heights from the surface to 135 km for the easterly QBO phase without OGW effects. One can see that the model reproduces basic features of the zonal jets in the troposphere and middle atmosphere. In the troposphere of the northern (winter) and the southern (summer) hemispheres, Fig. 1a demonstrates jets directed from the west to the east with maximum speed at latitudes of 30°–50° in both hemispheres. In the winter stratosphere, jet stream velocities maximize at altitudes about 60 km and latitudes 50°–70° N. In the summer stratosphere-mesosphere (southern hemisphere), zonal wind is directed westwards with maximum speed at altitudes 50–70 km. The structure of the zonal circulation presented in Fig. 1 and respective temperature fields calculated with the MUAM correspond quite well to the existing empirical standard models (e.g., Jacobi et al. 2009).

Figure 1 also presents the altitude-latitude structures of the monthly mean differences of zonal mean velocities due to inclusion of OGW effects for the easterly QBO phase (Fig. 1b) and differences between the westerly and easterly QBO phases without OGW effects (Fig. 1c) in January. In Fig. 1b, one can see the complicated structure of positive and negative velocity differences at the middle and high latitudes of the northern (winter) hemisphere at altitudes 30–100 km. Therefore, inclusion of OGW effects in the MUAM decreases the zonal wind maximum shown in Fig. 1a at altitudes 40–60 km and latitudes 50°–70° N and increases the maximum at altitudes 20°–40° N. This shifts the maximum of winter mesospheric jet stream in Fig. 1a southwards, which better corresponds to observations. The largest positive and negative zonal wind differences between the westerly and easterly QBO phases in Fig. 1c occur in the stratosphere near the equator. This is similar to the wind differences between the westerly and easterly QBO phases obtained from meteorological reanalysis data and simulated with tropospheric-stratospheric-mesospheric general circulation models by Yamashita et al. (2011) and Pogoreltsev et al. (2014). Our simulations cover altitudes

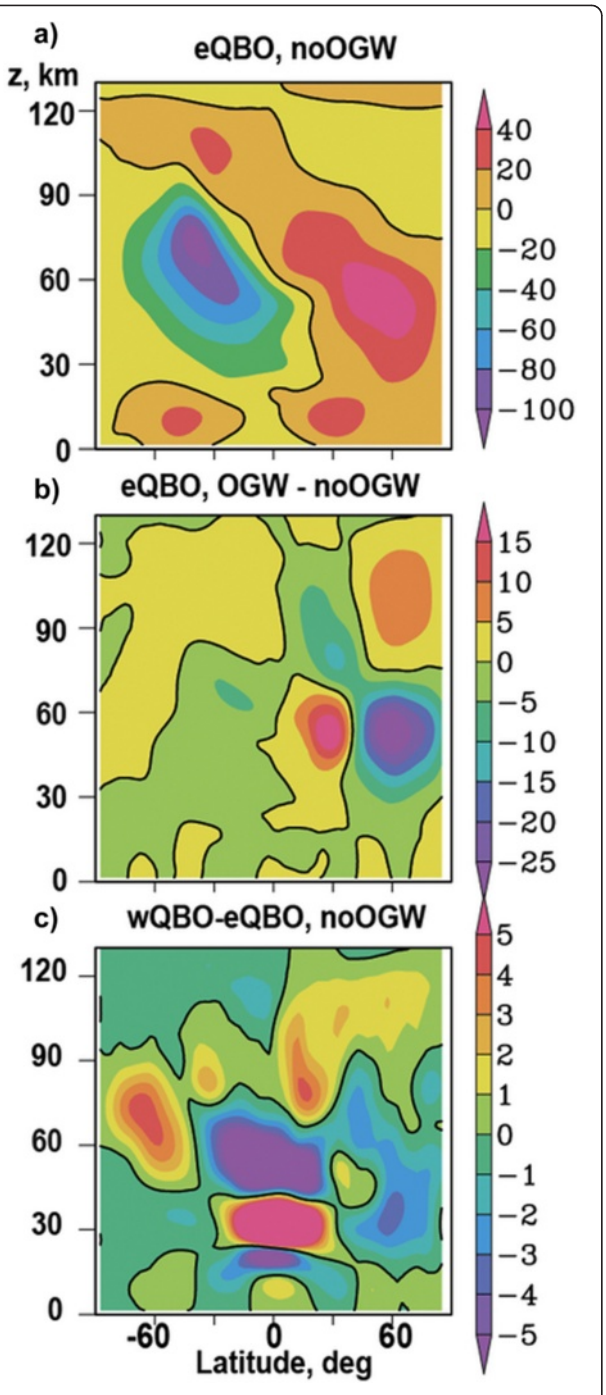

Fig. 1 Average for January zonal mean eastward velocity (m/s) for the easterly QBO phase without OGW effects **a** and velocity differences due to involving OGW effects in the easterly QBO phase **b** and due to change in QBO phase from easterly to westerly without OGW **c**. *Solid contours* correspond to zero values

up to 135 km and show zonal wind differences up to ±5 m/s in Fig. 1c in the middle and high latitudes of both hemispheres, showing the respective increases or decreases in zonal wind velocity during the westerly QBO phase compared to the easterly one.

As mentioned in "Methods," we made simulations for characteristics averaged for all Januaries with the westerly and easterly QBO phases during years 1992–2011. To verify the statistical confidence of nonzero differences in the mean winds in Fig. 1b, c, we can apply the statistical Student's t test (e.g., Rice 2006). From pairs of MUAM runs including and excluding OGW effects and for the easterly and westerly QBO phases during January at each latitude and altitude, we have for the comparison $87 \times 64 = 11{,}968$ pairs of velocities in grid nodes in time (4-h outputs) and longitude. We applied the paired t tests (Rice 2006) to these sets, which gave higher than 95 % confidences of nonzero monthly mean wind differences in 1559 of 1728 (90 %) grid points in latitude and altitude used for plotting Fig. 1c and similar results for Fig. 1b. Lesser than 95 % confidences were obtained only in regions where the absolute monthly mean wind differences are smaller than 0.1 m/s in Fig. 1b, c.

Inhomogeneities of the zonal wind velocity shown in Fig. 1a lead to different propagation conditions for the stationary OGWs. Figure 2a presents the average for January zonal mean OGW horizontal velocity amplitudes during the easterly QBO phase simulated with the parameterization of OGW effects (see "Methods"). Larger OGW amplitudes exist in the northern (winter) hemisphere because the reversal of summer global circulation in the strato-mesosphere (see Fig. 1a) produces critical levels for OGWs at altitudes about 20 km where zonal wind tends to zero (e.g., Gavrilov and Koval 2013). Using numerical simulations, Scinocca and Sutherland (2010) obtained similar results regarding the predominance of OGW amplitudes in the middle atmosphere of the winter hemisphere. Such increases in amplitudes of mesoscale waves in the strato-mesosphere of the winter hemisphere were observed in many experiments (Preusse et al. 2009; Gong et al. 2012; Gavrilov 2007). Figure 2b shows differences between OGW amplitudes calculated for the westerly and easterly QBO phases. During the westerly QBO phase, amplitudes of stationary OGWs are generally larger, especially at latitudes 30°–60° N, than that during the easterly QBO. The reasons for that could be differences in the mean zonal winds during the westerly QBO (see Fig. 1c), which can change effective vertical wavelengths of stationary OGWs, their dissipation, and conditions of wave propagation in the middle atmosphere.

OGW and QBO influence on planetary waves

To analyze the OGW and QBO phase impacts on planetary wave amplitudes, we performed the least squares longitude fitting of the calculated meteorological fields. We estimated the amplitudes of stationary planetary waves with zonal wavenumbers $m = 1$–4 and westward travelling NAMs, as it was suggested by Fedulina

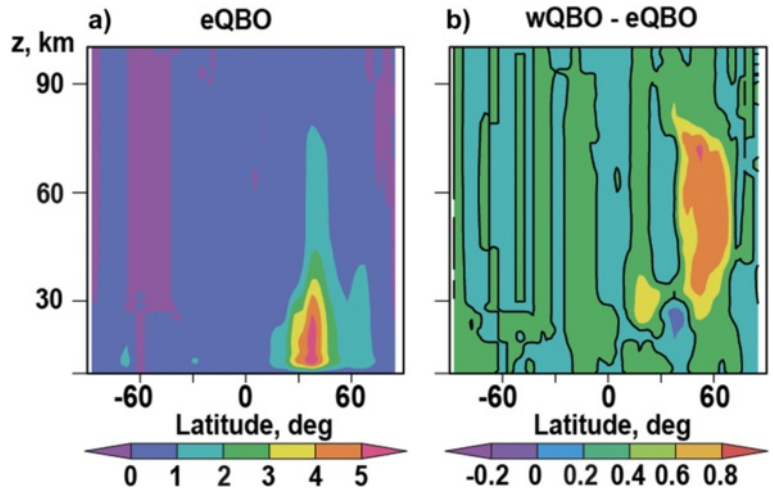

Fig. 2 January mean OGW velocity amplitudes (m/s) calculated for the easterly QBO phase **a** and the amplitude differences due to change in QBO phase from easterly to westerly **b**. *Solid contours* in panel **b** correspond to zero differences

et al. (2004). According to "Methods," we considered NAMs with periods of approximately 4, 5, 7, 10, and 16 days.

Figure 3a presents the monthly mean amplitudes of geopotential height variations caused by stationary PW modes with $m = 1–4$ (called as SPW1–SPW4 below). Figure 3a shows that in January SPWs have larger amplitudes in the northern (winter) hemisphere, where the seasonal zonal winds have the same directions at all altitudes. The SPW1 mode has maxima amplitudes at altitudes 40–70 km and latitudes 40°–70° N in the top panel of Fig. 3a. Amplitudes of SPW2–SPW4 in Fig. 3a have maxima in the troposphere-stratosphere and in the mesosphere at latitudes decreasing with the increase in m. Most SPW modes have secondary maxima at altitudes 80–100 km in the northern hemisphere. The bottom panels of Fig. 3a show smaller maxima of SPW3 and SPW4 amplitudes at low and high altitudes in the southern (summer in January) hemisphere.

Figure 3b shows the differences in SPW amplitudes in the easterly QBO phase after inclusion of OGW parameterization of dynamical and thermal effects into the MUAM. Positive or negative differences in Fig. 3b correspond to increases or decreases in the respective amplitudes after application of the OGW parameterization. Figure 3c shows similar differences of SPW amplitudes due to changes from easterly to westerly QBO phase without OGW effects. Student's t test show that nonzero differences of SPW amplitudes have 95 % statistical confidence, if their absolute values are larger than 3–5 gpm, which is valid for most parts of Fig. 3b, c.

For the easterly QBO phase, in Fig. 3b, one can see general decreases in the main maxima of SPW amplitudes in the middle atmosphere at middle latitudes of the northern hemisphere caused by OGW effects. Figure 3c reveals variations in SPW amplitudes due to changes from easterly to westerly QBO phases. It shows that variations of propagation conditions due to changes in tropical general circulation may lead to substantial changes in amplitudes of SPWs at the middle and high latitudes of the northern hemisphere (see below). The absolute peak values of SPW differences in Fig. 3b, c may reach 50–90 % and 30–70 % of maxima SPW amplitudes as shown in Fig. 3a at respective altitudes.

Figure 4a is similar to Fig. 3a and illustrates the amplitudes of the main westward travelling NAMs. It is noteworthy (see Fig. 4a) that 4- and 5-day NAMs have substantial amplitudes in both hemispheres due to their larger horizontal phase speeds and waveguides expanding to the southern (summer) hemisphere (see below). Other westward NAMs in Fig. 4a have the main amplitude maxima in the northern hemisphere. Considering the differences in westward NAM amplitudes due to OGW effects during the easterly QBO phase in Fig. 4b, one can conclude that the OGW influence leads to an increase in amplitudes (up to 90 %) of 4-day mode above 70 km in both hemispheres. The amplitudes of other westward NAMs in Fig. 4b show mixed increases and decreases at different altitudes and latitudes with the peak differences up to ±30–90 % from the peak amplitudes of respective NAMs in Fig. 4a in the northern hemisphere. Analysis of Fig. 4c reveals a general decrease (up to −50 %) in amplitudes of 5-day NAM above 40–50 km in both hemispheres due to change from the easterly to the westerly QBO phase and a general increase in amplitudes of 7- and 10-day waves.

Eliassen-Palm fluxes and refractivity indexes

Dickinson (1968) proposed the idea of the PW waveguide describing atmospheric regions where the background

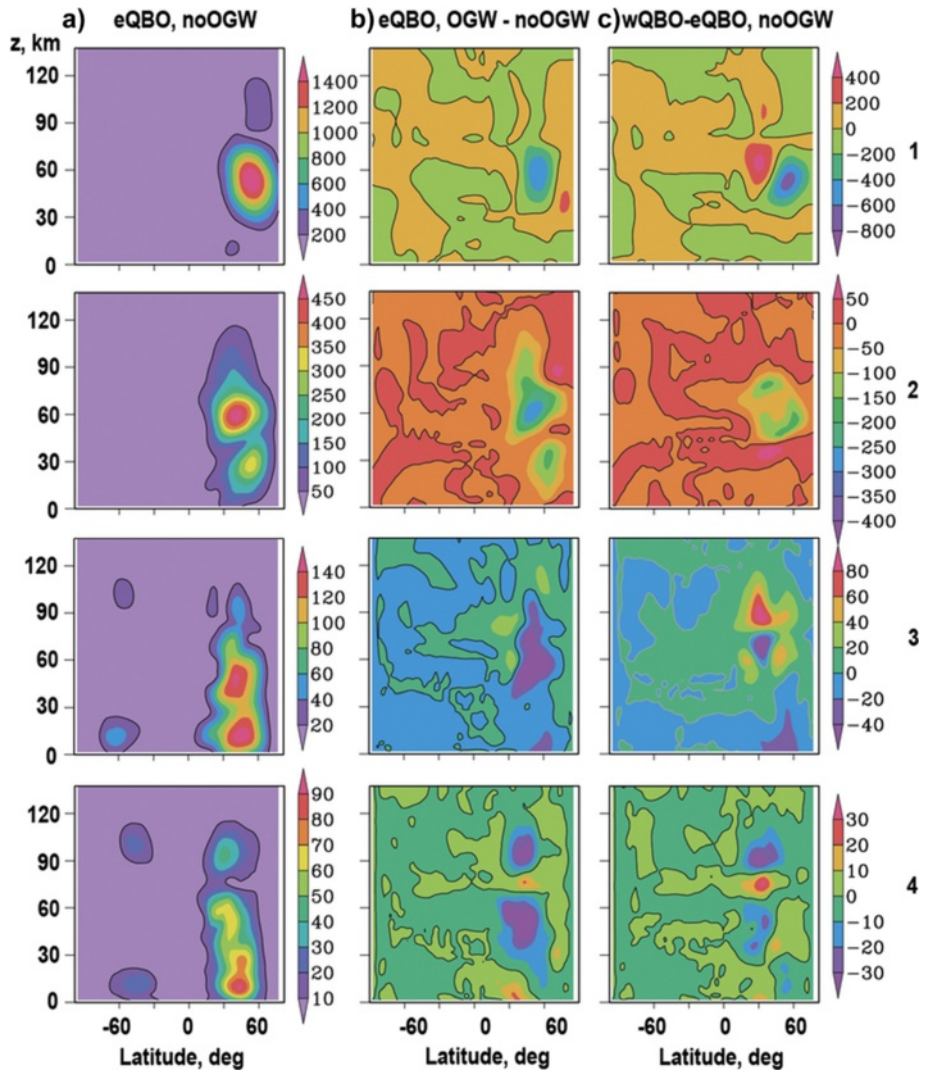

Fig. 3 January mean amplitudes of geopotential height variations (gpm) produced by stationary planetary wave modes with zonal wavenumbers *1*, *2*, *3*, and *4* (*panels* from the *top* to the *bottom*, respectively) for the easterly QBO phase without OGW effects **a**. The amplitudes differ due to involving OGW effects in the easterly QBO phase **b** and due to change in QBO phase from easterly to westerly without OGW **c**. *Solid contours* in panels **b** and **c** correspond to zero differences

wind and temperature allow wave propagation. Matsuno (1970) introduced the refractive index for PWs and found that the strongest PW propagation is in areas of large positive values of this index. To find out the influence of OGW effects and QBO phases on the PW waveguide, in this study, we use the expression for the quasi-geostrophic zonal mean refractive index squared, n_m^2, for the PW mode with zonal wavenumber m (Andrews et al. 1987; Karoly and Hoskins 1982; Li et al. 2007; Albers et al. 2013):

$$n_m^2(\phi, z) = \frac{\bar{q}_\phi}{\bar{u} - c} - \left(\frac{m}{a\cos\phi}\right)^2 - \left(\frac{f}{2NH}\right)^2, \qquad (3)$$

where $\bar{u}$ is the zonal mean zonal wind velocity; $\bar{q}_\phi$ is the latitudinal gradient of zonal mean potential vorticity; $c = 2\pi a\cos\phi/(m\tau)$ is the zonal phase velocity of PW mode; τ is the wave period, ϕ and z are the latitude and altitude, respectively; a is the Earth's radius, f is the Coriolis parameter, N is the Brunt-Väisälä frequency, and H is the atmospheric pressure scale height. For the potential vorticity $\bar{q}_\phi$ in Eq. (3), we use conventional formulae (e.g., Eq. (2) from Albers et al. 2013). According to the theory, PWs propagate in atmospheric regions where $n_m^2 > 0$ and should be evanescent in regions where $n_m^2 < 0$. Therefore, the PW waveguide extent is limited by the surfaces, where n_m^2 changes its sign. Frequently, these boundaries are located near PW critical levels, where $\bar{u} \to c$ and $|n_m^2| \to \infty$ according to Eq. (3). Considering changes in n_m^2, we can study the relative importance of the strength, shear, and

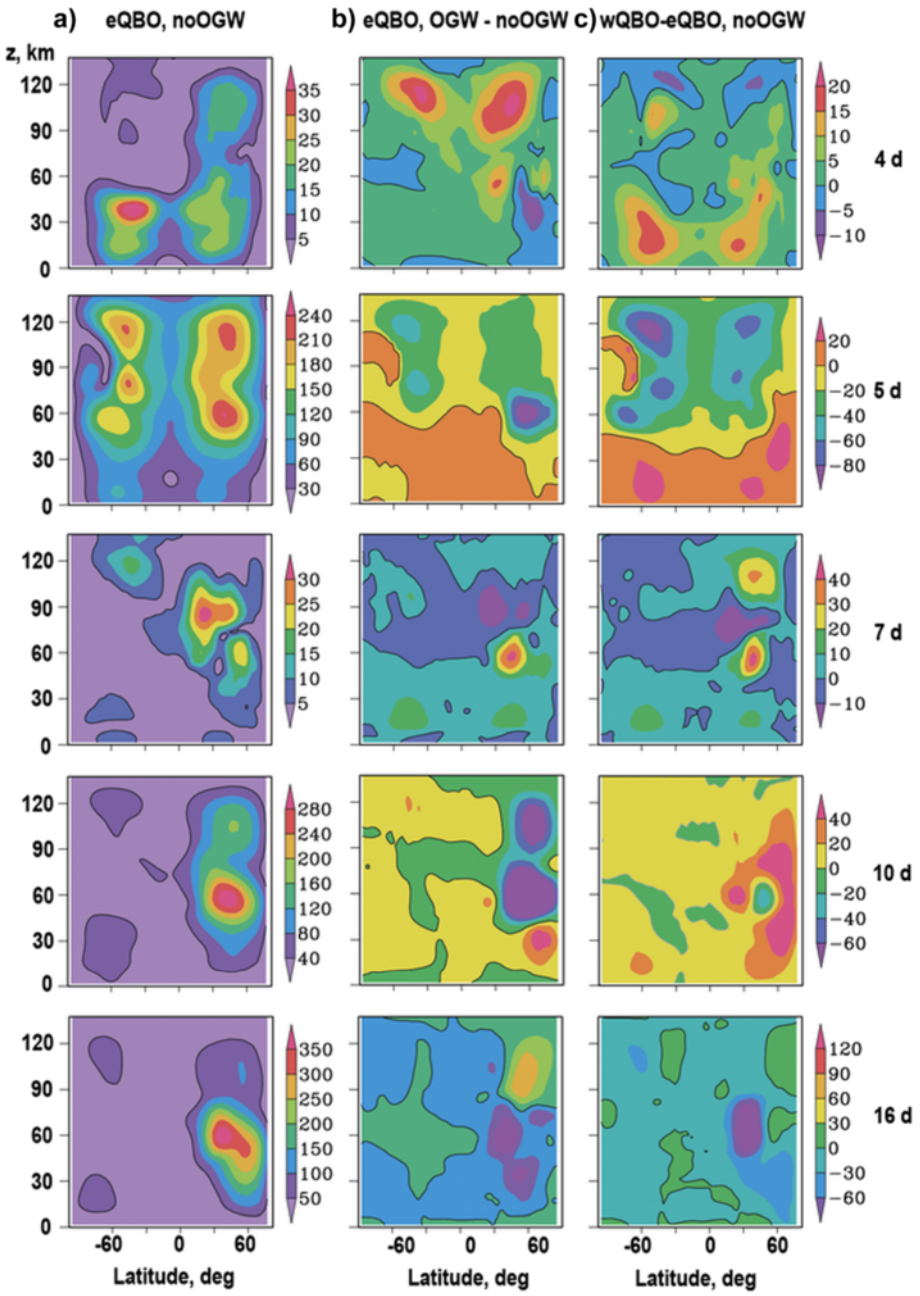

Fig. 4 a–c Same as Fig. 3 but for westward travelling normal atmospheric modes with periods *4*, *5*, *7*, *10*, and *16* days (*panels* from the *top* to the *bottom*, respectively) Figures 3 and 4 show that in many cases, accounting OGW dynamical and thermal effects in the MUAM results in changes in the amplitudes of stationary PWs and travelling NAMs. Depositions of OGW momentum and heat have primary effects directly modifying general circulation and planetary waves and secondary effects of influence of modified mean flow on the wave propagation conditions. Changes in the zonal wind direction in the middle atmosphere over the equator during different QBO phases modify the general circulation (see Fig. 1) and change PW and NAM propagation conditions. They can substantially affect PW amplitudes and other parameters up to higher altitudes described in some previous publications (Holton 1984; McLandress 2002; Ortland and Alexander 2006; Watanabe and Miyahara 2009; Mayr et al. 2011; Hoffmann et al. 2012). Inhomogeneities of orographic wave sources and conditions of OGW propagation may lead to the generation of additional PW modes, which could have contributed to the results in Figs. 3, 4, and 5 (e.g., Holton 1984; McLandress and McFarlane 1993; Watson and Gray 2015; Gavrilov et al. 2013b)

curvature of the zonal mean wind for the PW propagation. Eq. (3) shows that as the PW wavenumber m increases, n_m^2 decreases.

Another important PW characteristic is the Eliassen-Palm flux (EP-flux) vector $\boldsymbol{F_m} = \left(F_m^{(\phi)}, F_m^{(z)}\right)$. For quasi-geostrophic conditions and log-pressure vertical coordinate, the specific EP-flux components (divided by atmospheric density) are as follows (Andrews et al. 1987):

$$F_m^{(\phi)} = -a\cos\phi(\overline{u'v'}),\ F_m^{(z)} = af\cos\phi(\overline{v'\theta'})/\bar{\theta}_z, \qquad (4)$$

where primes denote perturbations produced by considered PW mode. According to Eq. (4), an upward direction of the EP-flux vector relates to the northward wave heat flux and the southward directed EP-flux vector relates to the northward PW momentum flux. The divergence of the EP-flux shows the net drag of the zonal mean flow by PWs. For example, negative values of the EP-flux divergence correspond to a westward drag on the mean wind.

For steady, slowly varying plane waves, the PW group velocity is parallel to the EP-flux vector. Additionally, the EP-flux vector $\boldsymbol{F_m}$ is curved up the gradient of n_m^2 and, particularly, is directed along ridges of n_m^2 (Palmer 1981, 1982; Karoly and Hoskins 1982). The magnitude of the EP-flux vector $|\boldsymbol{F_m}|$ is related to n_m^2 by (Palmer 1981, 1982):

$$\left|\vec{F}_m\right| = \psi_m^2 n_m^2/\left(2\rho_s af\right), \qquad (5)$$

where ψ_m is the amplitude of the considered PW mode and ρ_s is the surface density. Directions of the EP-flux vectors are inclined by gradients of n_m^2 $$ {n}_m^2 $$. Thus, n_m^2 $$ {n}_m^2 $$ and the EP-flux vector give a useful tool for visualizing the PW propagation conditions in the latitude-altitude plane.

Shaded areas in Fig. 5a show simulated latitude-altitude distributions of positive n_m^2 for stationary PWs with $m = 1$–4 in January in the easterly QBO phase. Their comparisons with Fig. 1a reveal correlations of PW waveguide with regions of positive zonal mean winds. Arrows in Fig. 6a show the specific EP-flux vectors of Eq. (4). They show that the main PW generation occurs at the middle latitudes of the winter hemisphere, where EP-fluxes are upwards at low latitudes and turn toward the equator at higher altitudes. This behavior is consistent with previous studies of EP-fluxes (Karoly and Hoskins 1982; Li et al. 2007; Inoue et al. 2011; Albers et al. 2013). Considerations of the different panels of Fig. 6a show that the largest EP-fluxes in the middle atmosphere are produced by SPW with $m = 1$. Increasing m in Fig. 6a leads to smaller magnitudes of EP-fluxes and their propagation up to smaller altitudes.

Different panels of Fig. 5b show differences in n_m^2 and EP-fluxes of SPWs caused by inclusion of the OGW effects into the numerical model. Positive and negative differences of the mean winds in Fig. 1b produce increases and decreases of n_m^2 in Fig. 6b. Changes in PW propagation conditions lead to differences in EP-flux vectors, shown with arrows in Fig. 6b. One can see that the main n_m^2 differences occur at altitudes 30–70 km and latitudes 20°–70° N, where OGW effects produce the largest changes in the zonal mean winds in Fig. 1b. In the top panel of Fig. 6a for SPW1, at altitudes 30–90 km, the difference vectors have the same directions as EP-fluxes in Fig. 5a at latitudes 0°–30° N and opposite directions at latitudes 30°–60° N. According to Eq. (3), increases in EP-flux magnitude may lead to increases in PW amplitudes, which can be observed in the top panel of Fig. 3b at altitudes 40–70 km and latitudes 30°–60° N. Decreasing EP-flux magnitudes and increasing n_m^2 in Eq. (3) correspond to decreasing SPW1 amplitudes at latitudes 30°–60° N and heights 30–70 km in the top panel of Fig. 3b.

Panels of Fig. 5b for $m > 1$ show dominance of the vector EP-flux differences directed opposite to the flux vectors in the respective panels of Fig. 6a at altitudes 30–70 km of the mid-latitude northern hemisphere. Decreasing EP-flux differences lead to the zones of negative differences of PW amplitudes in the respective panels of Fig. 3b, which span larger altitude ranges for shorter PWs with larger m.

Figure 5c reveals differences between n_m^2 and EP-fluxes under the westerly and easterly QBO phase conditions without inclusion of OGW effects. The main n_m^2 variations occur in the stratosphere at low latitudes, where the main QBO wind changes exist in the bottom panel of Fig. 1. In addition, Fig. 5c shows substantial n_m^2 changes in the middle and upper atmosphere at the middle and high latitudes of the northern hemisphere. In the top panel of Fig. 5c at altitudes 50–70 km, vectors of EP-flux differences have the same directions as the fluxes in the top panel of Fig. 5a at latitudes 20°–50° N and opposite direction at higher latitudes. Respective increases and decreases of EP-flux magnitudes form increases and decreases in SPW1 amplitudes in the top panel of Fig. 3c. For the PWs with $m > 1$, Fig. 6c shows vectors of EP-flux differences directed generally opposite to the flux vectors in the respective panels of Fig. 6a at the middle and high latitudes of the northern hemisphere. Respective EP-flux decreases in combination with n_m^2 changes, according to Eq. (5), produce increases and decreases of PW amplitudes seen in the panels of Fig. 5c for $m > 1$.

Figure 6a reveals n_m^2 and EP-fluxes for westward travelling NAMs for the easterly QBO phase without

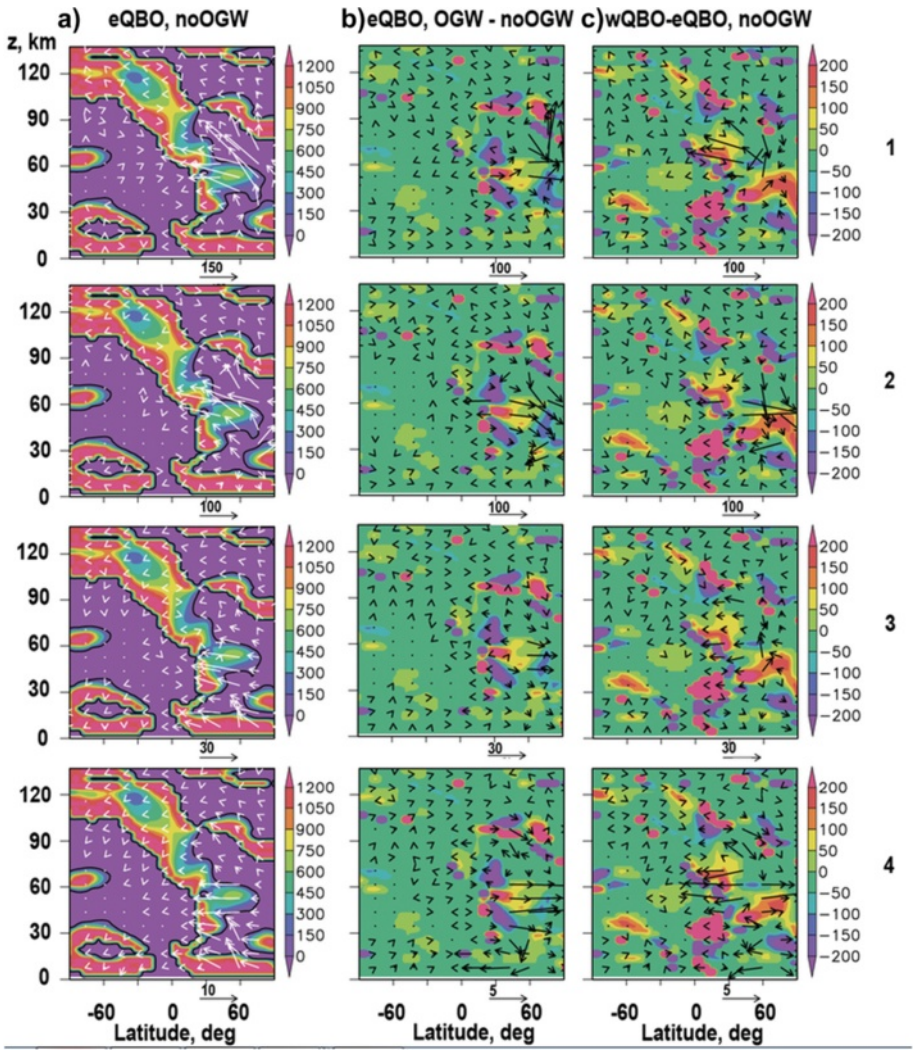

Fig. 5 January mean normalized refractive indexes $a^2 n_m^2$ (*shading*) and specific EP-fluxes in m^3/s^2 (*arrows*) produced by stationary planetary wave modes with zonal wavenumbers *1*, *2*, *3*, and *4* (*panels* from the *top* to the *bottom*, respectively) for the easterly QBO phase without OGW effects **a**. Also, $a^2 n_m^2$ and vector EP-flux differences due to involving OGW effects in the easterly QBO phase **b** and due to change in QBO phase from easterly to westerly without OGW **c**. *Solid contours* correspond to zero $a^2 n_m^2$

inclusion of OGW effects. In this case, the phase velocity $c < 0$ in Eq. (3) and areas of $n_m^2 > 0$ can span to the summer (southern) hemisphere in Fig. 6a. EP-fluxes in Fig. 6a show that the main portion of westward travelling NAMs are generated in the mid-latitude northern hemisphere, but then their energy can propagate to PW waveguides with $n_m^2 > 0$ in the southern hemisphere. Therefore, westward NAM amplitudes have maxima in both hemispheres in Fig. 4a. The largest amplitudes in the southern hemisphere in Fig. 5a have 5- and 4-day NAMs with the smallest negative zonal phase velocities $c = -95$ and $c = -61$ m/s at the equator, respectively. Therefore, westward travelling NAMs with relatively short periods can provide effective dynamical coupling between different hemispheres in the middle atmosphere. The vertical components of EP-fluxes in the middle atmosphere of the northern hemisphere are generally positive in Fig. 6a. According to Eq. (4), this corresponds to northward directions of the wave heat fluxes, which can heat regions near the North Pole in winter and contribute to the evolution of the sudden stratospheric warming events.

Differences in n_m^2 and $\boldsymbol{F_m}$ for westward NAMs produced by OGW effects are shown in Fig. 6b. One can see regions of positive and negative n_m^2 differences in all panels of Fig. 6b, which lead to changes in EP-fluxes. The vectors of EP-flux differences in Fig. 6b can be directed along or opposite to the respective fluxes in

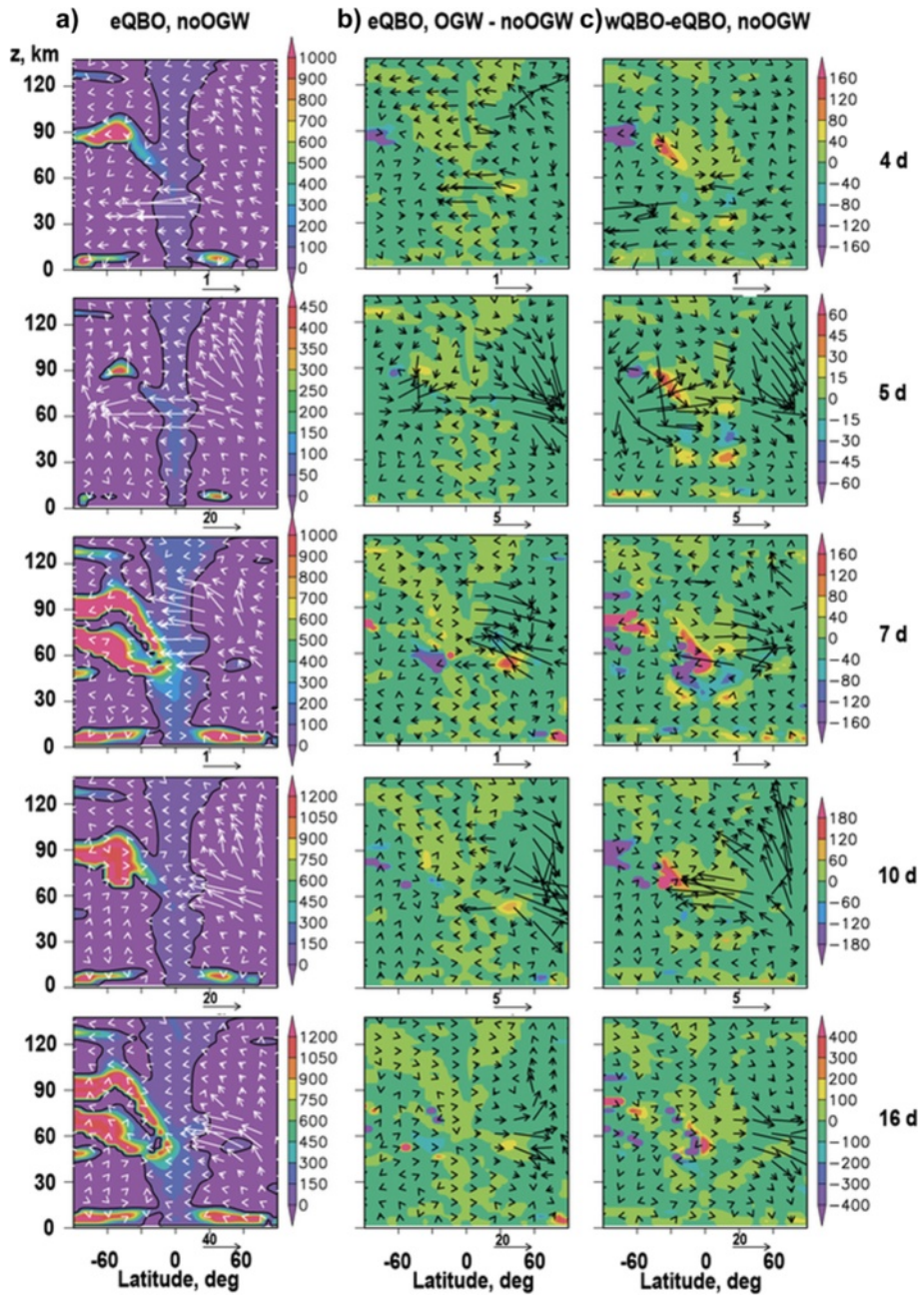

Fig. 6 a–c Same as Fig. 5 but for the westward travelling normal atmospheric modes with periods *4*, *5*, *7*, *10*, and *16* days (*panels* from the *top* to the *bottom*, respectively)

Fig. 6a. Therefore, differences in NAM amplitudes in Fig. 6b could be positive or negative depending on increases or decreases in EP-flux magnitudes. Differences of vertical EP-flux components in Fig. 6b in the middle atmosphere at latitudes 40°–90° N can be negative (see 5-, 10-, and 16-day waves) or positive (4- and 16-day waves above the altitude of 60 km and 7-day mode below 60 km), which correspond to additional cooling or heating of polar regions. Therefore, OGW influence propagation conditions of westward travelling NAMs could change thermal conditions in the middle atmosphere of winter Arctic.

Interesting features are increases in amplitudes of 4-day westward NAM in both hemispheres in the top panel of Fig. 4b at altitudes above 70 km. Considerations of the top panel of Fig. 6b reveal substantial increases in EP-fluxes directed at these altitudes across the equator from the northern to the southern hemisphere produced

by OGW effects for this mode. Combined with waveguides existing for 4-day westward NAM in the southern hemisphere in Fig. 6a, such increases in EP-fluxes can produce respective increases in amplitudes of this mode at high altitudes in the top panel of Fig. 4b.

Figure 6c reveals differences in n_m^2 and EP-fluxes between the years of westerly and easterly QBO phases. One can see that such differences exist in both hemispheres. Therefore, Fig. 5c shows changes in NAM amplitudes in both hemispheres, especially for 5- and 4-day westward modes having the strongest negative phase velocities. Signs of amplitude changes depend on signs of n_m^2 and EP-flux changes in Fig. 6c. For example, the top panel of Fig. 6c shows increasing poleward EP-fluxes in both hemispheres for 4- and 5-day westward NAMs at altitudes about 30 km during the westerly QBO phase, which corresponds to positive amplitude changes in the respective panels of Fig. 4c. Vector differences in EP-fluxes in Fig. 6c for 5-day mode have generally opposite directions to the fluxes in Fig. 6a at altitudes higher than 60 km. They decrease EP-flux magnitudes and form negative 5-day westward NAM amplitude changes in Fig. 4c in the middle atmosphere of both hemispheres. Most differences in vertical EP-flux components in Fig. 6c in the middle atmosphere at middle and high latitudes of the northern hemisphere have downward directions, which correspond to southward PW heat fluxes and cooling of the polar regions. For 10-day westward NAM in Fig. 6c, EP-fluxes are directed upwards in the northern hemisphere above altitude 30 km implying additional heating near the North Pole.

Figures 5 and 6 show that the changes in PW and NAM amplitudes shown in Figs. 3 and 4 could be associated with modifications in the mean wind, refractive index, and EP-flux structures produced by OGW dynamical and thermal effects and changes in QBO phases.

OGW drag modes

Time and spatial inhomogeneity of the mean wind drag produced by OGWs can be an additional mechanism of PW generation in the middle atmosphere (e.g., Holton 1984; McLandress and McFarlane 1993; Watson and Gray 2015). To study possible OGW drag influences, we decomposed simulated wave drags into herein considered stationary PW modes and travelling NAMs. For SPWs with $m = 1–5$ in January, amplitudes of OGW drag components are shown with shaded areas in the left panels of Fig. 7a. Arrows in Fig. 7a show differences in specific EP-fluxes due to OGW influence, which are the same as arrows in the respective panels of Fig. 6b.

Figure 7a shows that in the lower atmosphere, the maxima of stationary OGW drag components are located at latitudes of the main mountain systems of the northern and southern hemispheres. Westward wind systems in the middle atmosphere of the summer (southern) hemisphere prevent upward propagation of stationary OGW energy to high altitudes (see Fig. 2a). Hence, above 25–30 km maxima of OGW drag amplitudes in the left panels of Fig. 7a are located only in the winter (northern) hemisphere, mainly at latitudes 30°–50° N. The vertical structures of OGW drag depend on the vertical profiles of the mean wind and temperature (see Gavrilov and Koval 2013) and are different for different PW modes in Fig. 7a. Decreases in OGW drag amplitudes with altitude are larger for SPW modes with higher m in the left panels of Fig. 7a.

Arrows in Fig. 7a show changes in specific EP-flux vectors of stationary PW modes due to OGW effects. At latitudes higher than 30° N and altitudes 30–70 km, one can see northward EP-flux differences in all panels of Fig. 7a, which decrease EP-fluxes produced by tropospheric PW sources and plotted with arrows in Fig. 6a. They could be caused by OGW drag influence on the general circulation (see Fig. 1b) and PW refractive index (Fig. 6b), which modify the SPW propagation conditions in the middle atmosphere. Figure 7b reveals distributions of OGW drag amplitudes for westward travelling NAMs and respective differences in specific EP-flux vectors. General distributions of OGW drag components in Fig. 7b in the northern hemisphere are similar to those shown in Fig. 7a for SPWs. Significant changes in EP-fluxes in the regions of increased OGW drag components in Fig. 7b occur for 4-day westward NAM at altitudes about 90 km. The westward 4-day NAM has waveguides in the southern hemisphere (see Fig. 6a), which provide effective transfer of EP-fluxes into the summer hemisphere forming amplitude maxima at high altitudes in the top panel of Fig. 5a.

Therefore, OGW drag may directly alter local PW-fluxes or may indirectly change the general circulation of the middle atmosphere and the PW refractive indexes. Relative contributions of these effects depend on different stationary PW modes and travelling NAMs.

Discussion

Many studies were devoted to the generation of PW modes in the middle atmosphere by horizontally inhomogeneous gravity wave drag (e.g., Holton 1984; McLandress and McFarlane 1993; Watson and Gray 2015). Using the MUAM, Gavrilov et al. (2013a, b) simulated the generation of PW modes by inhomogeneous OGW forcing. In these simulations, tropospheric sources were given for stationary PWs only. Modeling showed the presence of westward travelling normal atmospheric modes (NAMs) produced by inhomogeneous OGW drag in the middle atmosphere. In the present study, we considered stationary PWs and travelling NAMs, whose main sources were specified in the troposphere. In this model, OGW drag could only

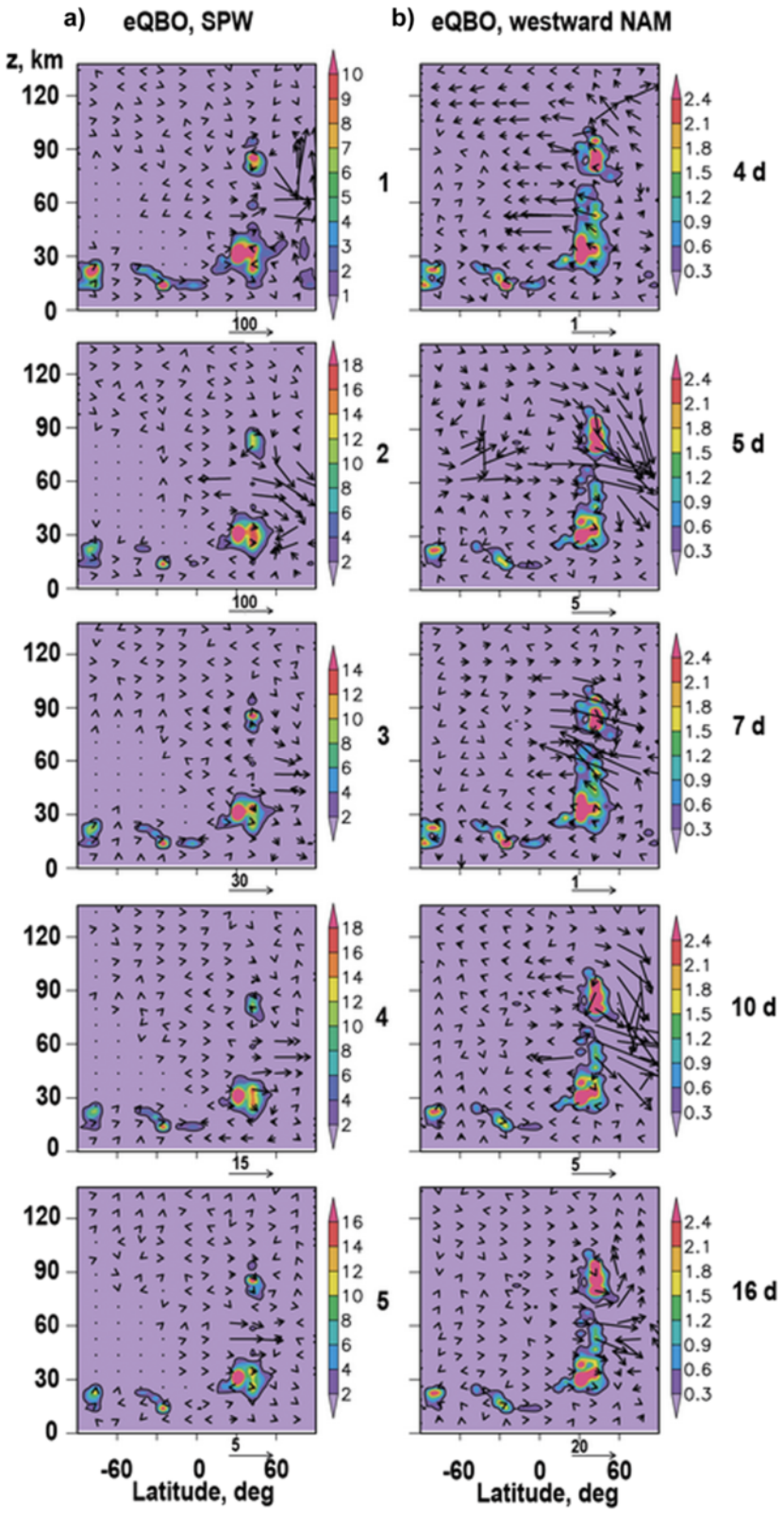

Fig. 7 January mean amplitudes of OGW drag components in 10^{-9} m/s^2 (*shading*) and respective changes in specific EP-fluxes in m^3/s^2 (*arrows*) for the easterly QBO phase and for stationary planetary wave modes with zonal wavenumbers *1–5* **a** and westward travelling NAMs **b**

modify the primary modes, while its relative contribution depends on the strengths of specified tropospheric PW sources.

Recently, some studies revealed possible compensation of PW drag of the middle atmospheric circulation by parameterized OGWs in general circulation models (McLandress and McFarlane 1993; Cohen et al. 2013, 2014; Sigmond and Shepherd 2014; Watson and Gray 2015). Our results show that taking account of OGW parameterization can both decrease or increase wave amplitudes, EP-fluxes, and wave drag of the mean flow depending on the considered PW modes. In Figs. 3b and 5b, amplitudes and EP-fluxes of stationary PWs decrease at latitudes higher than 30°–40° N in the middle atmosphere due to OGW effects. At lower latitudes, Figs. 3b and 5b show increases in amplitudes and EP-fluxes of SPW1 and SPW2 modes. Amplitudes and EP-fluxes of westward travelling NAMs in Figs. 4b and 6b are also increasing and decreasing at different latitudes and altitudes in the middle atmosphere. In addition to the direct impact of the wave drag, OGW can influence PW propagation conditions by changing background temperature and wind fields and modifying atmospheric refractive indexes (see Figs. 5 and 6). Combinations of inhomogeneous OGW drag and refractive index may produce quite complicated latitude-altitude distributions of amplitudes and EP-fluxes for different PW modes in the middle atmosphere.

Many studies are devoted to the role of PW-mean flow interactions in penetration of equatorial QBOs to the middle and high latitudes (e.g., Dunkerton and Baldwin 1991; O'Sullivan and Young 1992; Garfinkel et al. 2012; Lu et al. 2014). Some studies show that zonal wind velocity in the northern polar vortex can differ during the westerly QBO phase from that in the easterly phase (Holton and Tan 1980; Pascoe et al. 2005; Inoue et al. 2011; Yamashita et al. 2011; Watson and Gray 2014). Our simulated differences in the mean zonal winds between the westerly and easterly QBO phases at high latitudes of the northern hemisphere in Fig. 1c have different signs at different altitudes. In the troposphere and lower stratosphere, Fig. 1c shows higher eastward velocities at high latitudes of the northern hemisphere during the westerly QBO phase, which corresponds to the traditional Holton-Tan effect (Holton and Tan 1980; Inoue et al. 2011). Above altitude 30 km, Fig. 1c reveals increases and decreases in the mean zonal winds at middle and high latitudes during the westerly QBO phase. Some discrepancies between Fig. 1c and previous studies may arise from the MUAM deficiencies in the troposphere and lower stratosphere and from detection of QBO phases at different altitudes in different studies (see "Methods").

Possible mechanisms of equatorial QBO influence on the general circulation of the middle atmosphere include modifications of atmospheric waveguides, which can change conditions of the PW propagation and wave drag of the mean flow (e.g., Holton and Tan 1980; Inoue et al. 2011; Watson and Gray 2014). Figures 5c and 6c show that changes in the horizontal and vertical structures of background wind and temperature between westerly and easterly QBO phases can produce substantial differences in refractive indexes at the middle and high latitudes of both hemispheres in the middle atmosphere. These differences alter the propagation conditions of different PW modes and their amplitudes (see Figs. 3c and 4c) and EP-fluxes (see Figs. 5c and 6c) at middle and high altitudes. Respective changes in PW drag and heating rates can produce further changes in the general circulation and temperature at middle and high latitudes caused by changes in equatorial QBO phases in the middle atmosphere. The influences of background wind and temperature on refractive indexes and EP-fluxes of particular PW modes and NAMs can be different.

Therefore, our studies confirm existing views that nonlinear interactions between PW modes and general circulation could be important mechanisms of influence of tropical QBO phases on the dynamical and thermal regimes of the middle atmosphere at middle and high latitudes. Simulations also show that particular mechanisms and results of this influence may significantly depend on the parameters of the considered PW modes.

This study uses some simplified assumptions for parameterizations of OGW effects and travelling PW modes, for example, travelling PW modes treated as sinusoids with constant amplitudes versus time. Simulations are made for fixed distributions of NAM amplitudes and phases at the lower boundaries. Further studies of the OGW and QBO influence on tides and planetary waves with more realistic parameterizations are required.

Conclusions

The numerical simulations were performed using the MUAM with the implemented parameterization of dynamical and thermal effects of orographic gravity waves generated by the Earth's topography (Gavrilov and Koval 2013). Responses of the mean circulation and amplitudes of stationary and travelling planetary wave modes with periods of 4–16 days in the middle atmosphere to OGW impacts and to changes in the phase of the quasi-biennial oscillation were simulated. Accounting OGW dynamical and heating effects in the MUAM can lead to changes up to 50–90 % in the SPW amplitudes. Amplitudes of westward travelling NAMs can vary (up to 50–90 %) at different altitudes and latitudes of the northern hemisphere due to the OGW effects. PW and NAM amplitudes can have peak differences up to ±30–90 % at middle and high latitudes between the easterly and westerly QBO phases in tropics.

Analysis shows that obtained changes in PW amplitudes could be associated with modifications of the mean wind, refractive index, and EP-flux structures produced by OGW dynamical and thermal effects and changes in the QBO phases. Time and spatial inhomogeneities of OGW drag can lead to changes in EP-fluxes of stationary PWs and travelling NAMs. Our simulations confirm existing concepts that modifications of the extra-tropical general circulation of the middle atmosphere during the easterly and westerly QBO phases could be produced by changes in refractive indexes, PW propagation conditions, and subsequent PW drag of the mean flow. Details of these interactions are various for different stationary and travelling PW modes. Westward travelling NAMs may have extra-hemisphere waveguides and provide transfer of energy and momentum to the middle and upper atmosphere of the southern (summer) hemisphere.

Competing interests
The authors declare that they have no competing interests.

Authors' contributions
NMG supervised the work and participated in the simulations and in writing and drafting the manuscript. AVK made the numerical simulations with the MUAM and participated in drafting the manuscript. AIP participated in the improvements of the MUAM, NAM, and QBO parameterizations. ENS made the calculations of SPW amplitudes. All authors read and approved the final manuscript.

Acknowledgements
The work was supported by the Russian Science Foundation (#14-17-00685).

Author details
[1]Atmospheric Physics Department, Saint-Petersburg State University, Saint-Petersburg 198504, Russia. [2]Meteorological Forecast Department, Russian State Hydrometeorological University, Saint-Petersburg, Russia.

Received: 30 January 2015 Accepted: 29 May 2015
Published online: 10 June 2015

References
Albers JR, McCormack JP, Nathan TR (2013) Stratospheric ozone and the morphology of the northern hemisphere planetary waveguide. J Geophys Res Atmos 118:563–576. doi:10.1029/2012JD017937

Andrews DG, Holton JR, Leovy CB (1987) Middle atmosphere dynamics. Elsevier, New York

Baldwin MP, Gray LJ, Dunkerton TJ, Hamilton K, Haynes PH, Randel WJ, Holton JR, Alexander MJ, Hirota I, Horinouchi T, Jones DBA, Kinnersley JS, Marquardt C, Sato K, Takahashi M (2001) The quasi-biennial oscillation. Rev Geophys 39(2):179–229

Catry B, Geleyn JF, Bouyssel F, Cedilnik J, Broo R, Derková M, Mladek R (2008) A new sub-grid scale lift formulation in a mountain drag parameterisation scheme. Meteorol Zeitschrift 17(2):193–208

Cohen N, Gerber EP, Buhler O (2013) Compensation between resolved and unresolved wave driving in the stratosphere: implications for downward control. J Atmos Sci 70:3780–3798

Cohen N, Gerber EP, Buhler O (2014) What drives the Brewer-1 Dobson circulation. J Atmos Sci 71(10):3837–3855

Dickinson RE (1968) Planetary Rossby waves propagating vertically through weak westerly wave guides. J Atmos Sci 25:984–1002

Dunkerton TJ, Baldwin MP (1991) Quasi-biennial modulation of planetary-wave fluxes in the northern hemisphere winter. J Atmos Sci 48:1043–1061

Ebel A, Berger U, Krueger BC (1995) Numerical simulations with COMMA, a global model of the middle atmosphere. SIMPO Newsletter 12:22–32

Eckermann SD, Preusse P (1999) Global measurements of stratospheric mountain waves from space. Science 286:1534–1537

ETOPO2 (2015) Gridded global 2-minute relief data. National Geophysical Data Center, National Oceanic and Atmospheric Administration, U.S. Dept. of Commerce., http://www.ngdc.noaa.gov/mgg/global/etopo2.html. Accessed 11 Jun 2015

Fedulina IN, Pogoreltsev AI, Vaughan G (2004) Seasonal, interannual and short-term variability of planetary waves in UKMO assimilated fields. Q J Roy Meteorol Soc 130(602):2445–2458

Garfinkel CI, Shaw TA, Hartmann DL, Waugh DW (2012) Does the Holton-Tan mechanism explain how the quasi-biennial oscillation modulates the arctic polar vortex? J Atmos Sci 69:1713–1733

Gavrilov NM (2007) Structure of the mesoscale variability of the troposphere and stratosphere found from radio refraction measurements via CHAMP satellite. Izvestiya Atmos Oceanic Phys 43(4):451–460. doi:10.1134/S000143380704007X

Gavrilov NM, Fukao S (1999) Comparison of seasonal variations of gravity wave intensity observed with the middle and upper atmosphere radar with a theoretical model. J Atmos Sci 56(20):3485–3494. doi:http://dx.doi.org/10.1175/1520-0469(1999)056<3485:ACOSVO>2.0.CO;2

Gavrilov NM, Koval AV (2013) Parameterization of mesoscale stationary orographic wave impact for usage in numerical models of atmospheric dynamics. Izvestiya Atmos Oceanic Phys 49(3):244–251. doi:10.1134/S0001433813030067

Gavrilov NM, Pogoreltsev AI, Jacobi C (2005) Numerical modeling of the effect of latitude-inhomogeneous gravity waves on the circulation of the middle atmosphere. Izvestiya Atmos Oceanic Phys 41(1):9–18

Gavrilov NM, Koval AV, Pogoreltsev AI, Savenkova EN (2013a) Numerical simulation of the response of general circulation of the middle atmosphere to spatial inhomogeneities of orographic waves. Izvestiya Atmos Oceanic Phys 49(4):367–374. doi:10.1134/S0001433813040038

Gavrilov NM, Koval AV, Pogoreltsev AI, Savenkova EN (2013b) Numerical modeling influence of inhomogeneous orographic waves on planetary waves in the middle atmosphere. Adv Space Res 51(11):2145–2154. doi:10.1016/j.asr.2012.12.024

Gavrilov NM, Yudin VA (1992) Model for coefficients of turbulence and effective Prandtl number produced by breaking gravity waves in the upper atmosphere. J Geophys Res 97(D7):7619–7624. doi:10.1029/92JD00185

Geller MA, Zhou T, Ruedy R, Aleinov I, Nazarenko L, Tusnev NL, Sun S, Kelley M, Ye Cheng Y (2011) New gravity wave treatments for GISS climate models. J Clim 24:3989–4002. doi:10.1175/2011JCLI4013.1

Giorgetta MA, Bengtsson L, Arpe K (1999) An investigation of QBO signals in the east Asian and Indian monsoon in GCM experiments. Climate Dyn 15(6):435–450

Gong J, Wu DL, Eckermann SD (2012) Gravity wave variances and propagation derived from AIRS radiances. Atmos Chem Phys 12(4):1701–1720

Gossard EE, Hooke WH (1975) Waves in the atmosphere. Elsevier Sci. Publ. Co., Amsterdam-Oxford-New York

Hedin AE (1991) Extension of the MSIS thermospheric model into the middle and lower atmosphere. J Geophys Res 96:1159

Hoffmann P, Jacobi C, Borries C (2012) A possible planetary wave coupling between the stratosphere and ionosphere by gravity wave modulation. J Atmos Solar-Terr Phys 75–76:71–80. doi:10.1016/j.jastp.2011.07.008

Holton JR (1975) The dynamic meteorology of the stratosphere and mesosphere. Meteorol Monogr 15(37):1–218

Holton JR (1984) The generation of mesospheric planetary waves by zonally asymmetric gravity wave breaking. J Atmos Sci 41(23):3427–3430

Holton J, Tan H (1980) The influence of the equatorial quasibiennial oscillation on the global circulation at 50 mb. J Atmos Sci 37:2200–2208

Huesmann AS, Hitchman MH (2001) The stratospheric quasi-biennial oscillation in the NCEP reanalyses: climatological structures. J Geophys Res 106(D11):11859–11874. doi:10.1029/2001JD900031

Inoue M, Takahashi M, Naoe H (2011) Relationship between the stratospheric quasi-biennial oscillation and tropospheric circulation in northern autumn. J Geophys Res 116, D24115. doi:10.1029/2011JD016040

Jacobi C, Fröhlich K, Portnyagin Y, Merzlyakov E, Solovjova T, Makarov N, Rees D, Fahrutdinova A, Guryanov V, Fedorov D, Korotyshkin D, Forbes J, Pogoreltsev A, Kürschner D (2009) Semi-empirical model of middle atmosphere wind from the ground to the lower thermosphere. Adv Space Res 43:239–246

Jakobs HJ, Bischof M, Ebel A, Speth P (1986) Simulation of gravity wave effects under solstice conditions using a 3-d circulation model of the middle atmosphere. J Atmos Terr Phys 48:1203–1223

Jiang JH, Wu DL, Eckermann SD (2002) Upper Atmosphere Research Satellite (UARS) observation of mountain waves over the Andes. J Geophys Res 107(D20):8273. doi:10.1029/2002JD002091
Karoly DJ, Hoskins BJ (1982) Three dimensional propagation of planetary waves. J Meteor Soc Japan 60:109–123
Kelley MC (1997) Aspects of weather and space weather in the Earth's upper atmosphere: the role of internal atmospheric waves vol. 6. Int. Sci. Lect. Ser. Nat. Acad. Press, Washington, D.C, pp 1–31
Kim YJ, Arakawa A (1995) Improvement of orographic gravity wave parameterization using a mesoscale gravity wave model. J Atmos Sci 52(11):1875–1902
Krismer TR, Giorgetta MA (2014) Wave forcing of the quasi-biennial oscillation in the Max Planck Institute Earth System Model. J Atmos Sci 71:1985–2006
Li Q, Graf H-F, Giorgetta MA (2007) Stationary planetary wave propagation in Northern Hemisphere winter—climatological analysis of the refractive index. Atmos Chem Phys 7:183–200
Longuet-Higgins MS (1968) The eigenfunctions of Laplace's tidal equation over a sphere. Philos T R Soc Lond 262:511–607
Lott F, Miller MJ (1997) A new subgrid-scale orographic drag parametrization: its formulation and testing. Quart J Roy Meteorol Soc 123:101–127
Lu H, Bracegirdle TJ, Phillips T, Bushell A, Gray L (2014) Mechanisms for the Holton-Tan relationship and its decadal variation. J Geophys Res Atmos 119:2811–2830. doi:10.1002/2013JD021352
Matsuno T (1970) Vertical propagation of stationary planetary waves in the winter Northern Hemisphere. J Atmos Sci 27:871–883
Mayr HG, Mengel JG, Chan KL, Huang FT (2011) Middle atmosphere dynamics with gravity wave interactions in the numerical spectral model: tides and planetary waves. J Atmos Solar-Terr Phys 73:711–730
McLandress C (2002) The seasonal variation of the propagating diurnal tide in the mesosphere and lower thermosphere. Part I: the role of gravity waves and planetary waves. J Atmos Sci 59:893–906
McLandress C, McFarlane NA (1993) Interactions between orographic gravity wave drag and forced stationary planetary waves in the winter northern hemisphere middle atmosphere. J Atmos Sci 50(13):1966–1990
O'Sullivan D, Young RE (1992) Modeling the quasi-biennial oscillation's effect on the winter stratospheric circulation. J Atmos Sci 49:2437–2448
Ortland DA, Alexander MJ (2006) Gravity wave influence on the global structure of the diurnal tide in the mesosphere and lower thermosphere. J Geophys Res 111:A10S10. doi:10.1029/2005JA011467
Palmer TN (1981) Aspects of stratospheric sudden warmings studied from a transformed Eulerian-mean viewpoint. J Geophys Res 86:9679–9687
Palmer TN (1982) Properties of the Eliassen-Palm flux for planetary scale motions. J Atmos Sci 39:992–997
Pascoe CL, Gray LJ, Crooks SA, Juckes MN, Baldwin MP (2005) The quasi-biennial oscillation: analysis using ERA-40 data. J Geophys Res 110, D08105. doi:10.1029/2004JD004941
Phillips DS (1984) Analytical surface pressure and drag for linear hydrostatic flow over three-dimensional elliptical mountains. J Atmos Sci 41:1073–1084
Pogoreltsev AI (1999) Simulation of planetary waves and their influence on the zonally averaged circulation in the middle atmosphere. Earth Planets Space 51(7/8):773–784
Pogoreltsev AI (2007) Generation of normal atmospheric modes by stratospheric vacillations. Izvestiya Atmos Ocean Phys 43(4):423–435
Pogoreltsev AI, Vlasov AA, Froehlich K, Jacobi C (2007) Planetary waves in coupling the lower and upper atmosphere. J Atmos Solar-Terr Phys 69:2083–2101. doi:10.1016/j.jastp.2007.05.014
Pogoreltsev AI, Kanukhina AY, Suvorova EV, Savenkova EN (2009) Variability of planetary waves as a signature of possible climatic changes. J Atmos Solar-Terr Phys 71:1529–1539. doi:10.1016/j.jastp.2009.05.011
Pogoreltsev AI, Savenkova EN, Pertsev NN (2014) Sudden stratopheric warmings: the role of normal atmospheric modes. Geomagn Aeron 54(3):387–403. doi:10.7868/S0016794014020163
Preusse P, Dornbrack A, Eckermann SD, Riese M, Schaeler B, Bacmeister JT, Broutman D, Grossman KU (2002) Space-based measurements of stratospheric mountain waves by CRISTA: 1. Sensitivity, analysis method, and a case study. J Geophys Res 107(D23):8178. doi:10.1029/2001JD000699
Preusse P, Eckermann SD, Ern M (2009) Global ray tracing simulations of the SABER gravity wave climatology. J Geophys Res 114, D08126. doi:10.1029/2008JD011214
Rice JA (2006) Mathematical statistics and data analysis, 3rd edn. Duxbury Press, Belmont
Scinocca JF, McFarlane NA (2000) The parameterization of drag induced by stratified flow over anisotropic orography. Quart J Roy Meteorol Soc 126(568):2353–2393
Scinocca JF, Sutherland BR (2010) Self-acceleration in the parameterization of orographic wave drag. J Atmos Sci 67(8):2537–2546
Sigmond M, Shepherd TG (2014) Compensation between resolved wave driving and parameterized orographic gravity wave driving of the Brewer–Dobson circulation and its response to climate change. J Clim 27(14):5601–5610
Smith S, Baumgardner J, Mendillo M (2009) Evidence of mesospheric gravity-waves generated by orographic forcing in the troposphere. Geophys Res Lett 36, L08807. doi:10.1029/2008GL036936
Suvorova EV, Pogoreltsev AI (2011) Modeling of nonmigrating tides in the middle atmosphere. Geomagmetizm and Aeronomy 51(1):105–115
Swarztrauber PN, Kasahara A (1985) The vector harmonic analysis of Laplace's tidal equations. SIAM J Sci Stat Comp 6:464–491
Swinbank R, O'Neill A (1994) Stratosphere-troposphere assimilation system. Mon Weather Rev 122:686–702
Vosper SB, Brown AR (2007) The effect of small-scale hills on orographic drag. Quart J Roy Meteorol Soc 133:1345–1352
Watanabe S, Miyahara S (2009) Quantification of the gravity wave forcing of the migrating diurnal tide in a gravity wave–resolving general circulation model. J Geophys Res 114, D07110. doi:10.1029/2008JD011218
Watson PAG, Gray LJ (2015) The stratospheric wintertime response to applied extratropical torques and its relationship with the annular mode. Clim Dyn 44:2513–2537
Watson PAG, Gray LJ (2014) How does the quasi-biennial oscillation affect the stratospheric polar vortex? J Atmos Sci 71(1):391–409
Yamashita Y, Akiyoshi H, Takahashi M (2011) Dynamical response in the Northern Hemisphere midlatitude and high-latitude winter to the QBO simulated by CCSR/NIES CCM. J Geophys Res 116, D06118. doi:10.1029/2010JD015016